

Graphene Size-Dependent Multifunctional Properties of Unidirectional Graphene Aerogel/Epoxy Nanocomposites

Ne Myo Han,[†] Zhenyu Wang,[†] Xi Shen,[†] Ying Wu,[†] Xu Liu,[†] Qingbin Zheng,^{†,‡} Tae-Hyung Kim,[§] Jinglei Yang,[†] and Jang-Kyo Kim^{*,†}

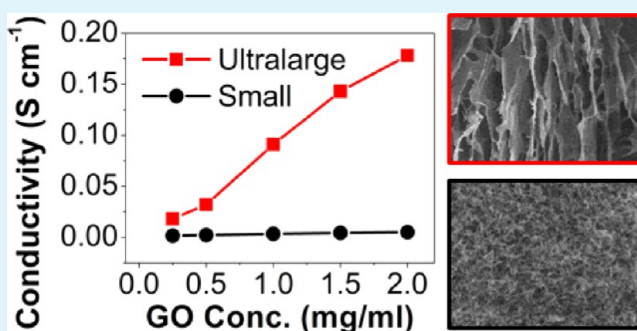
[†]Department of Mechanical and Aerospace Engineering and [‡]Institute for Advanced Study, The Hong Kong University of Science and Technology, Clear Water Bay, Kowloon, Hong Kong

[§]Integrative Research Center for Two-Dimensional Functional Materials, Institute of Interdisciplinary Convergence Research, Chung-Ang University, Seoul 06974, Republic of Korea

Supporting Information

ABSTRACT: Unidirectional graphene aerogels (UGAs) with tunable densities, degrees of alignment, and electrical conductivities are prepared by varying the average size of precursor graphene oxide (GO) sheets between 1.1 and 1596 μm^2 . UGAs prepared using ultralarge GO (UL-UGA) outperform those made from small GO in these properties. The UL-UGA/epoxy composites prepared by infiltrating liquid epoxy resin into the porous UGA structure exhibit an excellent electrical conductivity of 0.135 S/cm, along with an ultralow percolation threshold of 0.0066 vol %, which is one of the lowest values ever reported for all graphene-based composites. Owing to their three-dimensional interconnected network, a high degree of alignment, and effective reduction, UL-UGAs effectively enhance the fracture toughness of epoxy by 69% at 0.11 vol % graphene content through unique toughening mechanisms, such as crack pinning, crack deflection, interfacial debonding, and graphene rupture. These aerogels and composites can be mass-produced thanks to the facile, scalable, and cost-efficient fabrication process, which will find various multifunctional applications.

KEYWORDS: graphene aerogel, size effect, epoxy composites, percolation threshold, fracture toughness



1. INTRODUCTION

Electrically conductive polymer composites offer a wide range of applications, such as strain sensors,^{1–3} actuators,^{4–6} energy storage,^{7,8} electromagnetic interference (EMI) shielding devices,^{9–11} and electronic devices.^{7,12} Conductive polymer composites are commonly prepared by incorporating conductive fillers, such as metal wires,¹³ carbon black (CB),^{14–16} carbon nanotubes (CNTs),^{17–19} and graphene,^{20,21} into insulating polymer matrices. With increasing amount of conductive fillers in the polymer matrix, the composites undergo an insulator-to-conductor transition, as characterized by a sharp increase in electrical conductivity on the formation of a percolated network. Composites with low percolation thresholds are highly desired as they are cost-effective and retain the useful properties of the polymers. Such composites may be obtained by utilizing fillers with high aspect ratios and good electron mobility, such as two-dimensional (2D) graphene. However, the performance of graphene/polymer composites is often hindered by the inherent difficulty to uniformly disperse individual graphene sheets within the viscous polymer matrix. To ameliorate these issues, graphene sheets may be grown or assembled into three-dimensional (3D) interconnected structures, such as graphene foams (GFs), by

chemical vapor deposition (CVD),^{22,23} or graphene aerogels (GAs), by freeze-drying, prior to mixing with the polymer matrix. GAs are commonly prepared by self-assembly of graphene oxide (GO) sheets at a high temperature and pressure to form graphene hydrogels, which are subsequently freeze-dried to replace the aqueous medium with atmospheric air.^{24–26} GAs prepared using this method possess excellent mechanical flexibility, but failed to show ultralow densities due to the inevitable stacking of GO sheets during self-assembly. More recently, GAs with ultralow densities and highly aligned microstructures have been synthesized via direct freeze-drying of GO dispersions, in which ice crystals were used as the template for GO sheet assembly.^{27,28}

As GAs are able to maintain interconnected networks of conductive reduced GO sheets during the preparation of composites, their densities directly affect the percolation threshold of the resulting composites. Thus, to achieve a low percolation threshold, it is imperative to design a GA assembly with a minimum density that could maintain a stable structure

Received: December 15, 2017

Accepted: February 1, 2018

Published: February 1, 2018

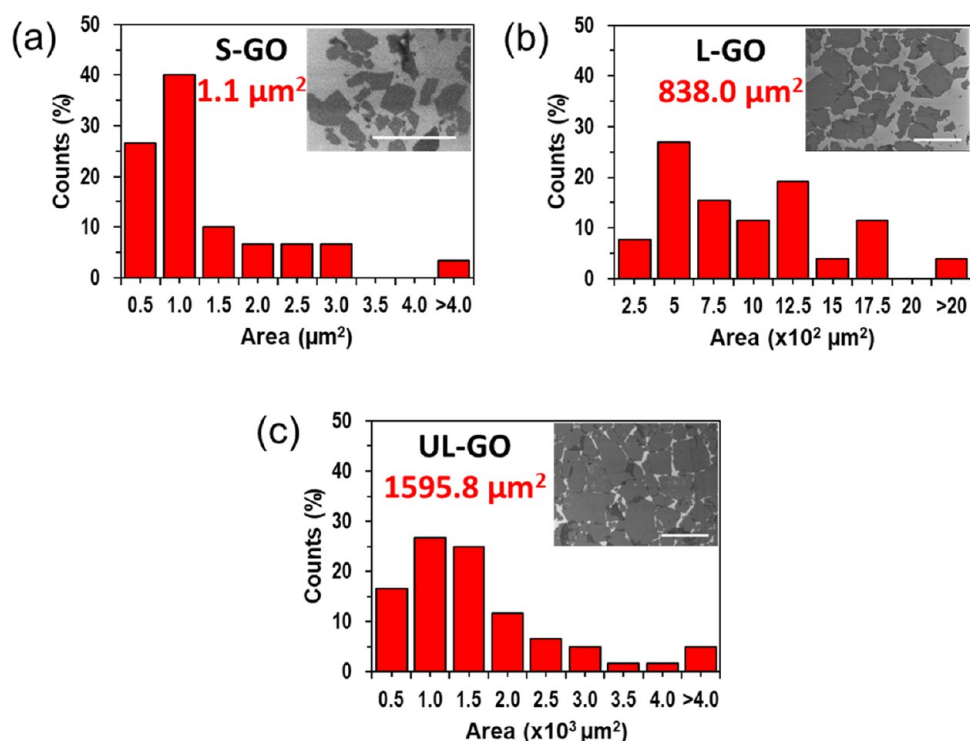


Figure 1. GO size distribution of sorted S-GO, L-GO, and UL-GO. The insets show typical SEM images for each size group, with scale bars of $5 \mu\text{m}$ for (a) and $50 \mu\text{m}$ for (b, c).

and exhibit the desired properties, i.e., high electrical conductivity. Precise control of the GA microstructure requires optimization of self-assembly conditions of GO sheets under freeze casting. In particular, the freezing temperature plays an important role in determining the porous structure: for example, casting at $-196 \text{ }^\circ\text{C}$ produced GAs with small cellular pores ($10 \mu\text{m}$) and thin pore walls (20 nm), whereas freezing at $-10 \text{ }^\circ\text{C}$ resulted in GAs with large lamellar pores ($800 \mu\text{m}$) and thick pore walls ($80 \mu\text{m}$).²⁹ The GO concentration has also shown to directly influence GA pore size, which varied from 40 to $10 \mu\text{m}$ with increasing GO concentration from 1.83 to 14.0 mg/mL .³⁰ Another important parameter to consider when designing 3D graphene structures, the size of the precursor material, is often overlooked. The size of graphene sheets has shown to influence important mechanical, physical, optical, and transport properties of various graphene assemblies and their composites. In particular, large graphene sheets produced stronger graphene assemblies and composites with better electrical, optoelectronic, and moisture barrier characteristics than those prepared using smaller graphene sheets.^{31–34} A recent theoretical study also predicts that the minimum density of 3D graphene assemblies was inversely proportional to the size of their building blocks.³⁵ The gelation of GO sheets, a critical phenomenon in the formation of aerogel, also depends largely on their size.³⁶ However, the effect of graphene sheet size on the assembly of GO sheets and properties of GAs has yet to be established.

In this work, we demonstrate the positive effect of large GO size on the morphological, physical, and mechanical properties of the resulting unidirectional graphene aerogels (UGAs) and the epoxy composites reinforced with UGAs. It is found that the UGAs prepared using ultralarge GO (UL-UGA) sheets exhibited much lower densities, higher degrees of alignment, and higher electrical conductivities than those prepared using

small GO (S-UGA) sheets of the same amount. The composites fabricated by infiltrating liquid epoxy into the porous UL-UGAs retained higher electrical conductivities with a significantly lower percolation threshold than the S-UGA counterparts did. The experimental percolation thresholds were validated by an interparticle distance percolation model taking into account the GO size and alignment. Interestingly, the UL-UGAs were shown to effectively enhance the fracture toughness of epoxy composites by introducing toughening mechanisms that are absent in the composites with S-UGAs.

2. EXPERIMENTAL SECTION

2.1. Fabrication of UGAs and UGA/Epoxy Composites. GO was produced from natural graphite flakes (supplied by Asbury Graphite Mills) using the modified Hummers method³⁷ and sorted into three different size groups through a two-step centrifugation. To prepare UGAs, the GO dispersion was first frozen in a polypropylene tube using liquid nitrogen (see Figure S2) and freeze-dried for 48 h (Labconco FreeZone, $-105 \text{ }^\circ\text{C}$, 10 Pa) to form GA. The GA was thermally annealed in air at $200 \text{ }^\circ\text{C}$ for 2 h and reduced at $900 \text{ }^\circ\text{C}$ in a N_2 atmosphere for 2 h to produce conductive UGA. Epoxy resin (LY 1556, supplied by Huntsman Advanced Materials) and curing agent (XB 3471, supplied by Huntsman Advanced Materials) were mixed at a weight ratio of 100:12 and infiltrated into the UGA under vacuum for 2 h. The composite mixture was cured at $80 \text{ }^\circ\text{C}$ for 30 min and post-cured at $110 \text{ }^\circ\text{C}$ for 2 h to produce solid UGA/epoxy composites. It should be noted that for electrical conductivity measurement the difference in graphene content used for different GO sizes was inherent to the variation in UGA density with GO size and concentration, as explained in Section S2.

2.2. Characterization and Mechanical Tests. Scanning electron microscopy (SEM, JEOL 6390F) was used with an accelerating voltage of 20 kV to characterize GO size, as detailed in Section S1 in Supporting Information, UGA alignment, and UGA/epoxy fracture surface. A nitrogen adsorption device (Coulter SA3100) was used to obtain the adsorption/desorption isotherms of UGAs at 77 K . X-ray photoelectron spectroscopy (XPS, Axis Ultra DLD) was used to study

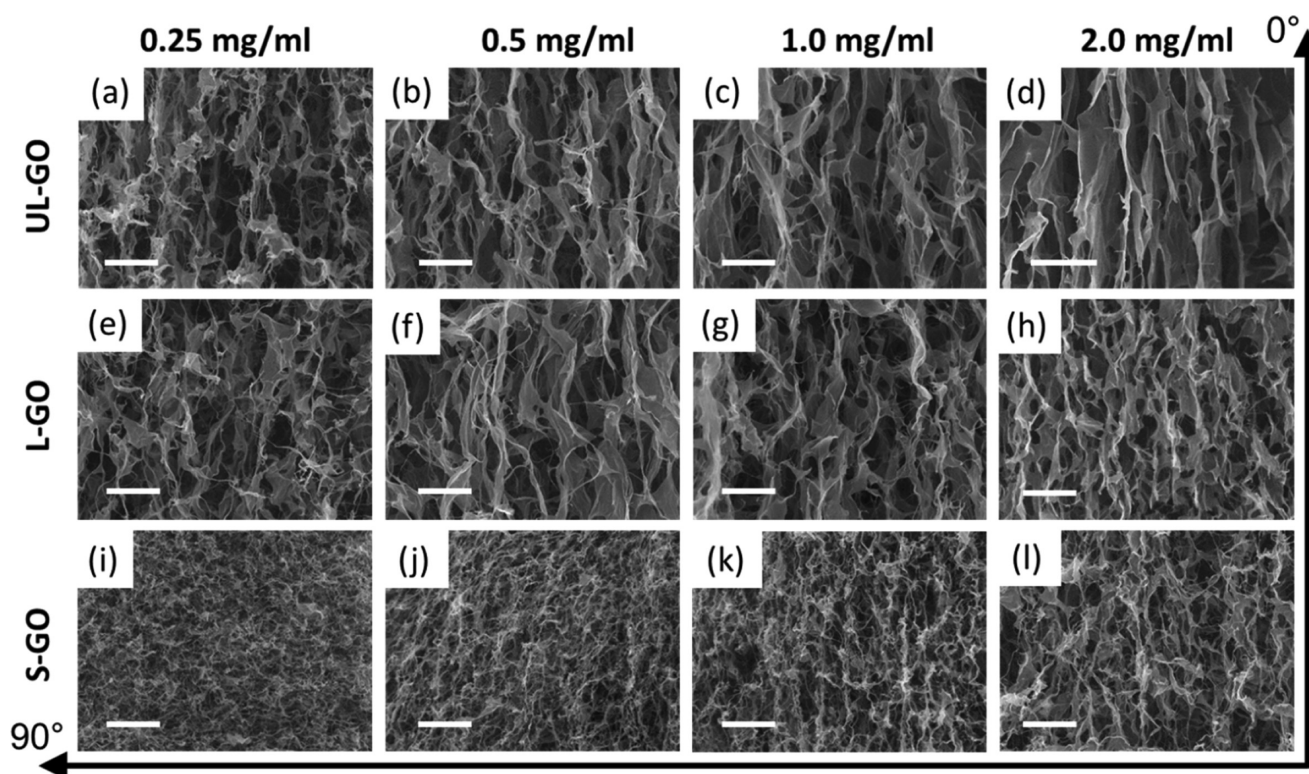


Figure 2. Typical SEM images showing vertical cross sections of UGAs prepared using (a–d) UL-GO, (e–h) L-GO, and (i–l) S-GO, with varying concentrations of 0.25–2.0 mg/mL. All scale bars represent 50 μm , and the arrow pointing to 0° indicates the ice growth direction.

the elemental compositions of UGAs. Raman spectroscopy (Reinshaw MicroRaman) was used to characterize the optical resonance of GO, UGAs, and UGA/epoxy using a He–Ne laser (632.8 nm) at 10% (2.5 mW) power. A four-point probe (Scientific Equipment & Services) was used to measure the electrical conductivities of UGA and UGA/epoxy composites. The universal testing machine (MTS Alliance RT/05) was used to measure the flexural strength and modulus of UGA/epoxy composites using 28 mm long \times 3 mm wide \times 1.6 mm thick flexural samples in three-point bending with a support span of 24 mm and a crosshead speed of 2.0 mm/min, according to the specification, ASTM D790. The mode I fracture toughness of UGA/epoxy composites was measured using 28 mm long \times 6 mm wide \times 3 mm thick edge-notched bending samples with a support span of 24 mm and a crosshead speed of 10.0 mm/min, according to the specification, ASTM D5045.

3. RESULTS AND DISCUSSION

3.1. Size Distribution of Sorted GO Sheets. Among different GO preparation methods, chemical oxidation of expanded graphite obtained by thermal shock expansion of graphite intercalation compounds has been reported to produce high yield of large-size GO dispersions.³⁷ To prepare GO dispersions with different sheet sizes, a two-step centrifugation method was used to obtain three GO size groups. The average areas of GO sheets for each size group, small GO (S-GO), large GO (L-GO), and ultralarge GO (UL-GO), were 1.1, 838.0, and 1595.8 μm^2 , respectively, as shown in Figure 1. The huge size differences between them were sufficient to observe the size effect on the properties of graphene assemblies.

3.2. Morphologies of UGAs. The unidirectional freeze casting technique was used to fabricate aligned porous polymers, ceramics, and metals by utilizing a single temperature gradient to control the ice crystal growth and particle ejection direction.³⁸ Unlike spherical zero-dimensional (0D) materials,

one-dimensional (1D) multiwalled CNTs (MWCNTs) and two-dimensional (2D) graphene can produce 3D assemblies with porosities higher than 99% due to their high aspect ratios and significant particle interactions.³⁹ UGAs were prepared by unidirectional freeze-casting of GO dispersion, followed by thermal reduction,²⁸ as shown in Figure S2 along with digital images of the as-prepared aerogels.

To study the degree of alignment and porosity of UGAs, the concentration and size of GO sheets were varied, and the inner morphologies of the resulting UGAs are shown in Figure 2. The UGAs prepared using L- and UL-GO exhibited vertically aligned graphene pore walls with a consistent pore width of around 20–30 μm . These pore walls were connected by bridges oriented perpendicular to them.²⁸ The UGAs prepared using UL-GO at low concentrations (Figure 2a,b) had relatively thin and loosely connected pore walls composed of few layers of graphene. This is an example of the desired morphology when designing a polymer composite with a low percolation threshold, as the intrinsic 3D interconnected structure of UGA guarantees a path for electrical conduction, whereas the few layers of graphene in the pore walls minimize the filler content of the composite. As the precursor GO concentration was increased, the resulting UGAs showed an increasing degree of alignment and better-defined pore wall thickness (Figure 2c,d). In contrast to UL-UGAs, S-UGAs presented almost random orientations with much lower degrees of alignment regardless of the precursor graphene concentration (Figure 2i–l).

The degree of alignment of UGA pore walls was quantitatively evaluated using the software Image Pro Plus (Media Cybernetics, Inc.) and their SEM images.³² The acute angle formed between the freezing direction and each observable graphene pore wall was measured and compiled to

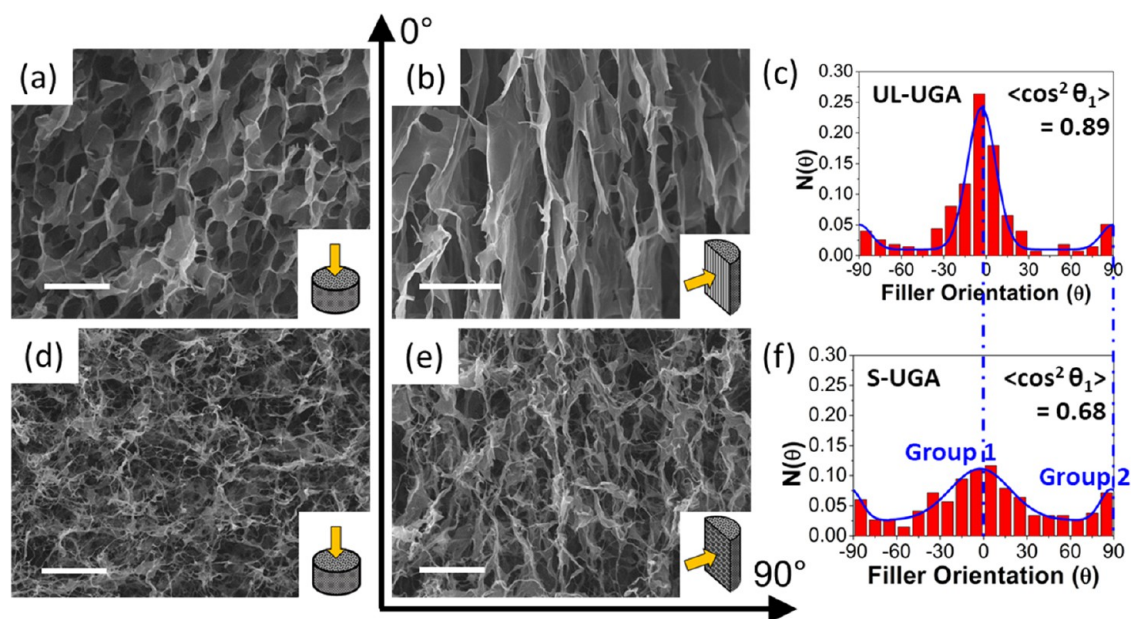


Figure 3. Typical SEM images showing (a) horizontal and (b) vertical cross sections of UGAs fabricated with 2.0 mg/mL UL-GO and (d) horizontal and (e) vertical cross sections of UGAs fabricated with 2.0 mg/mL S-GO. Filler orientation distributions and $\langle \cos^2 \theta_1 \rangle$ values of (c) UL-UGA and (f) S-UGA. All scale bars represent 50 μm , and the arrow pointing to 0° indicates the ice growth direction.

form a distribution histogram, in which the fraction of graphene sheets within each 10° interval, labeled $N(\theta)$, was plotted against the filler orientation, θ . Such histograms for UL-UGA and S-UGA are shown in Figure 3c,f, respectively. The bimodal distribution displayed by the histograms, with peaks centered at 0 and 90°, portrayed the prevalence of vertically aligned graphene walls and horizontal graphene bridges, respectively. The degree of graphene alignment in the UGA structure was quantified by calculating the mean orientation factor, $\langle \cos^2 \theta \rangle$, on the basis of the orientation distribution (see Section S3, Supporting Information), and the results are given in Figure 3c,f. It is worth noting that UL-UGAs had a high $\langle \cos^2 \theta_1 \rangle$ value of 0.89, which approaches unity and signifies highly aligned graphene sheets in the vertical direction. In contrast, S-UGA had a much lower $\langle \cos^2 \theta_1 \rangle$ value of 0.68, close to $\langle \cos^2 \theta_1 \rangle = 0.5$, representing randomness of the structure with poor orientation in 2D space. These values were in good agreement with the visual observations from the SEM images and served as important parameters in determining theoretical percolation thresholds.

Apart from the variation in degree of alignment, a variation in pore size was also observed, contrary to the UGAs fabricated with the same freezing parameters in a previous report.²⁹ UGAs prepared using S-GO at a low concentration (Figure 2i) had in general smaller pores than those fabricated with larger GO sheets or the same-size GO sheets at higher concentrations. There was a significant shrinkage of the whole S-UGA structure during the freeze drying process, which was mainly responsible for the shrunken pore size. The following mechanism, represented schematically in Figure 4a, is proposed on the basis of the GO aspect ratio and intersheet interactions. During the unidirectional freeze casting process, the vertical ice crystals squeezed the GO sheets between them to form the pore walls. In the case of UL-UGA, there were sizeable interactions, namely, hydrogen bond, steric hindrance, π - π interaction, and van der Waals forces,^{32,33,40} between adjacent UL-GO sheets to align them within the pore walls. Upon drying, a few UL-GO

sheets having comparable sizes to the pores may align perpendicular to the pore walls to support the overall 3D structure, resulting in graphene bridges. Meanwhile, for S-UGA, there were limited interactions between the neighboring S-GO sheets due to their small sizes, as shown in Figure 4b. The XPS image of S-GO shown in Figure 4c presents a slightly higher fraction of carboxyl group ($-\text{COOH}$ at 289.0 eV) but lower fractions of hydroxyl ($-\text{C}-\text{OH}$ at 286.9 eV) and carbonyl/epoxy ($-\text{C}=\text{O}/\text{C}-\text{O}-\text{C}$ at 287.7 eV) groups than UL-GO. According to the Lerf-Klinowski model, the $-\text{COOH}$ group exists at the edges, whereas the $-\text{C}-\text{OH}$ and $\text{C}-\text{O}-\text{C}$ groups are found on the basal planes of GO sheets.⁴¹ Because of their smaller sizes, S-GO sheets have higher perimeter/area ratios than UL-GO sheets, resulting in a higher fraction of $-\text{COOH}$ group but lower fractions of $-\text{C}-\text{OH}$ and $\text{C}-\text{O}-\text{C}$ groups. Experimental and simulation results have shown that the $-\text{C}-\text{OH}$ group contributed to significant face-to-face interaction between GO sheets and enhanced alignment of UL-GO sheets (Figure 4b).^{32,33} As a result, the pore walls in S-UGA were not rigid enough to maintain the original aligned structure during the drying process, causing significant shrinkage and random orientation of UGA after collapse, as seen in Figure S3. Although the same was observed for all UGAs prepared using S-GOs, the degree of shrinkage decreased with increasing GO concentration, evident from the larger pores (see Figure 2i vs Figure 2j). The sheer amount of GO sheets available to form the pore walls may have compensated for the limited interactions between the sheets.^{24,36} This might reduce the shrinkage effect, but was insufficient to enhance their alignment.

3.3. Physical Properties and Chemical Attributes of UGAs. The properties of pore walls of UGAs were further examined by their nitrogen adsorption/desorption isotherms, as shown in Figure 5a. The existence of hysteresis loops (type IV isotherm) for both UL-UGA and S-UGA evidenced the occurrence of capillary condensation, suggesting the presence of mesoporous pore walls. The shapes of these hysteresis loops

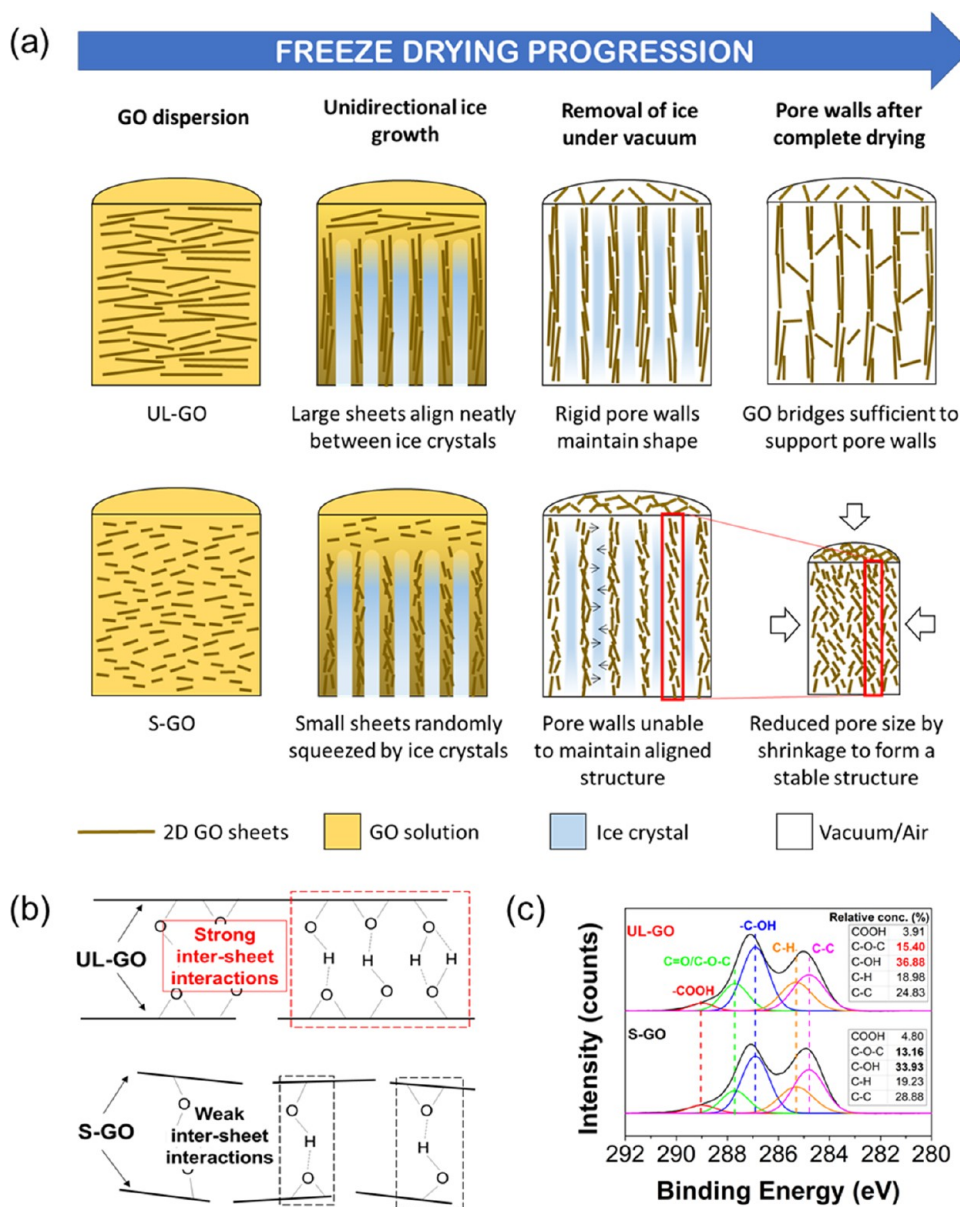


Figure 4. (a) Schematic of freeze drying progression of aerogels prepared using UL-GO and S-GO and (b) comparison of intersheet interactions in the form of hydrogen bonds between GO sheets. (c) XPS deconvoluted C 1s spectra of UL-GO and S-GO, showing relative concentrations of each carbon-containing group.

presented information on pore shape: the two branches of the hysteresis loop for UL-UGA were relatively horizontal and parallel at high P_s/P_0 values, which best matched the type H4 loop, indicating the presence of narrow, slit-shaped pores.⁴² On the other hand, the S-UGA had a wider loop and relatively vertical branches, which matched the type H3 loop usually observed for aggregates of platelike particles.⁴² Furthermore, the Brunauer–Emmett–Teller surface area and the total pore volume of UL-UGA were remarkable, 560 m²/g and 1.76 cm³/g, respectively, which are considerably higher than 207 m²/g and 1.08 cm³/g of S-UGA (Figure 5a,b). These findings suggest that during the freeze drying process, S-GO sheets tended to aggregate to greater extents than UL-GO sheets did, validating the aforementioned observations and mechanisms (Figures 2 and 4a).

XPS was used to characterize the degree of reduction in GO after thermal treatment. The deconvoluted C 1s spectra of UL-

GO were characterized by the abundant hydroxyl (–C–OH at 286.9 eV) functional groups and sp² graphitic (C–C at 284.8) domain, as shown in Figure 5c. Additionally, there were trace peaks of carboxyl (–COOH at 289.0 eV), carbonyl/epoxy (–C=O/C–O–C at 287.7 eV), and carbon–hydrogen (C–H at 285.3 eV) functional groups. These functional groups contributed to the interactions among UL-GO sheets to form rigid, aligned pore walls.^{32,33} After thermal reduction, the spectra for UL-UGA exhibited drastic changes with elimination of oxygen-containing peaks, suggesting that the reduction process effectively removed the oxygenated functional groups from the aerogel.⁴³ The O 1s peak almost entirely disappeared, leading to a surge of the corresponding C/O ratio from 2.64 to 53.9. In addition, the Raman spectra given in Figure 5d presented a reduction in intensity ratio of the D- to G-bands, I_D/I_G , from 2.36 to 1.51 and downshifts of both the D- and G-band peaks after reduction. These modifications signify the

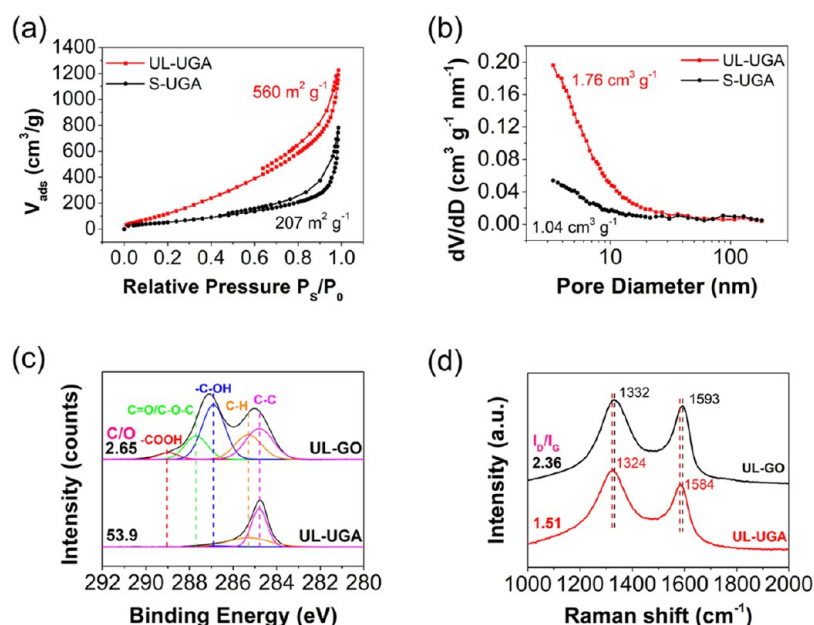


Figure 5. (a) Nitrogen adsorption/desorption isotherms and (b) adsorption pore size distribution of UL-UGA and S-UGA. (c) XPS deconvoluted C 1s spectra and (d) Raman spectra of UL-GO and UL-UGA. All UGAs were prepared using GO dispersions of 1.0 mg/mL concentration.

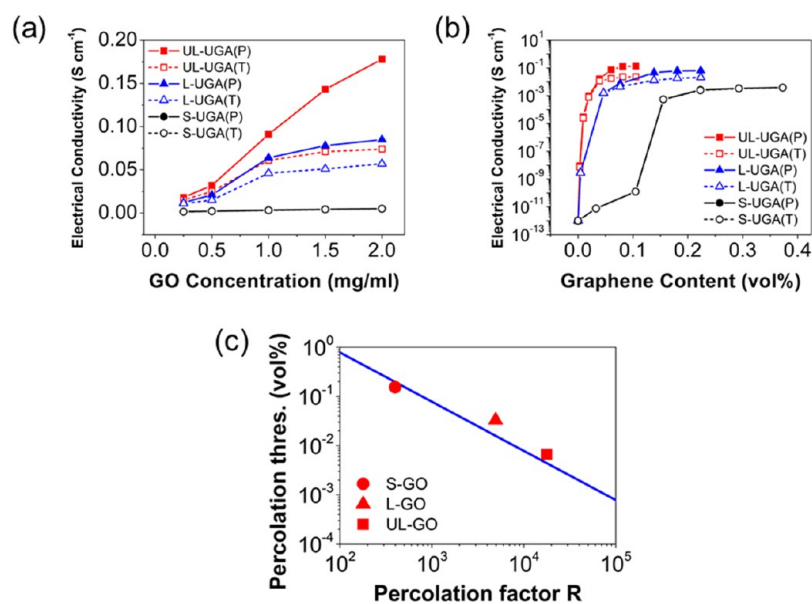


Figure 6. Electrical conductivities of (a) UGAs prepared using different GO concentrations and (b) UGA/epoxy composites with different graphene contents, measured parallel (P) and transverse (T) to the graphene sheet alignment. (c) Comparison of percolation thresholds between theory (blue line) and experiments (red symbols).

recovery of sp^2 graphitic structure due to the removal of functional groups.⁴⁴ The above findings prove that the thermal reduction process was effective in reducing GO, which may give rise to enhanced electrical conductivities and mechanical properties of the aerogels and the resulting composites to be discussed below.

For comparison, the matching XPS and Raman spectra of S-GO and S-UGA are shown in Figure S4. As previously stated, the XPS image of S-GO presented a slightly higher fraction of $-COOH$ but lower fractions of $-C-OH$ and $C-O-C$ groups than UL-GO, due to its smaller size and the relative position of each group on the graphene sheet according to the Lerf-Klinowski model.⁴¹ Meanwhile, the Raman spectra of UL-GO and UL-UGA presented a lower I_D/I_G ratio than those of S-GO

and S-UGA, attributed to the fewer edge defects present in larger GO sheets. Furthermore, UL-UGA displayed a lower G-band peak position at 1584 cm^{-1} than S-UGA at 1586 cm^{-1} , also signifying fewer defects in the larger graphene sheets.⁴⁴

3.4. Electrical Properties of UGAs and UGA/Epox Resin Composites. Composites prepared using 3D graphene structures offer at least two primary benefits compared to those using 2D graphene sheets,⁴⁵ namely, (i) the elimination of filler dispersing steps and (ii) the assurance of conductive networks within the polymer matrices. UGAs, having such a 3D structure, enjoy these benefits along with exceptionally low percolation thresholds in composites due to the inherently interconnected network, where the percolation threshold is simply limited by the density of the precursor material. By

Table 1. Comparison of Percolation Thresholds of Carbon Nanofiller/Epoxy Composites

filler	processing method	aspect ratio of filler	percolation threshold (vol %)	conductivity near percolation (S/cm)	ref
0D Carbon Black					
CB	shear mixing; adding CuCl ₂	~1	0.3; 0.06	10 ⁻⁵	50
CB	shear mixing	~1	~2.7	10 ⁻⁵	51
1D Carbon Nanotubes					
MWCNT	sonication, stirring	100	0.02	10 ⁻³	53
MWCNT	ultraviolet–ozone treatment, sonication	80–160	0.0031	2 × 10 ⁻⁸	56
MWCNT	shear mixing	200; 860	0.0014; 0.0025	10 ⁻⁶ ; 10 ⁻⁷	54
SWCNT	sonication	400	0.0052	10 ⁻⁹	55
2D Graphene and rGO					
rGO	sonication, stirring	~250	0.52	10 ⁻⁹	57
rGO	in situ polymerization	~15 000	0.12	10 ⁻⁷	45
pristine graphene	freeze drying, mixing	1000–1667	0.088	10 ⁻⁸	20
3D Graphene Network					
GF	CVD, vacuum infiltration		0.027	~1	23
GA	hydrogen iodide reduction, freeze drying	~16 000	0.14	10 ⁻⁷	25
UGA	unidirectional freezing, vacuum infiltration	~16 000	0.007	10 ⁻⁴	28
UL-UGA	unidirectional freezing, vacuum infiltration	~31 600	0.0066	10 ⁻⁵	current study

freeze-drying GO dispersions with progressively lower concentrations, UGAs with thinner pore walls and lower densities may be prepared, down to a point where there would be insufficient GO sheets to assemble and support a continuous 3D network.³⁵

The electrical conductivities of UGAs and UGA/epoxy composites are shown in Figure 6a,b. Across all GO sizes, the conductivity increased consistently with increasing GO concentration or graphene content by having denser pore walls with thicker graphene layers.^{24–26} UGAs fabricated using 2.0 mg/mL of UL-GO sheets exhibited an electrical conductivity of 0.178 S/cm along the alignment direction, whereas the corresponding UGA/epoxy composites had an electrical conductivity of 0.135 S/cm at 0.11 vol % of UL-UGA. If each corresponding pair of data points are compared, the conductivities of UGA/epoxy composites were only slightly lower than those of the respective UGA reinforcements. This means that the vacuum-assisted epoxy infiltration was a suitable method to prepare the composites, as it damaged little of the interconnected graphene networks and was able to preserve the electrical conductivity of the composites along the alignment direction. The conductivities of UGAs prepared using larger GO sheets were significantly higher than those prepared using smaller sheets, due to a lower total intersheet resistance within the interconnected graphene network.¹⁸ The electrical conductivities of L-UGA, UL-UGA, and their composites, measured transverse to the graphene alignment direction were lower than those along the alignment direction. These disparities arose from the anisotropic nature of the UGA graphene networks prepared by unidirectional freeze casting (see Figure 2). In addition, the infiltration of epoxy resin caused a large reduction in conductivity along the transverse direction. This observation may be caused by the displacement or breakage of the thin graphene bridges linking the graphene walls by the liquid epoxy resin during the infiltration process,²⁸ giving rise to highly anisotropic electrical conductivities: 0.135 S/cm along the parallel direction versus 0.023 S/cm along the transverse direction in the UL-UGA/epoxy composite. In comparison, S-UGAs and their composites had similar conductivities in the two orthogonal directions because their

graphene sheets were not well aligned and inherently random with no apparent anisotropy.

A similar trend in anisotropic behavior was also observed in the Raman spectra of UGA/epoxy composites (Figure S7). The intensities of the Raman spectra obtained in the two orthogonal directions were similar in the case of S-UGA/epoxy composites, whereas those for the UL-UGA/epoxy composites were significantly higher in the alignment direction than in the transverse direction. The direction-dependent Raman peak intensity meant that there was signal resonance by graphene sheets parallel to the laser and suppression by those perpendicular to it.⁴⁵ Such observations validate the potential use of UGA and UGA/epoxy composites in multifunctional applications that benefit from anisotropic properties, such as anisotropic conductors and EMI shielding devices.^{46–48}

The percolation thresholds of the UGA/epoxy composites fabricated with S-UGA, L-UGA, and UL-UGA were 0.154, 0.033, and 0.0066 vol %, respectively, as determined using the power law equation described in Section S4. Large differences in percolation threshold were expected because larger GO sheets have the intrinsic ability to form an interconnected 3D network at a lower filler content due to their higher aspect ratios than the smaller GO sheets. To validate the relationship between GO size and the percolation threshold of corresponding composites, the percolation thresholds of UGA/epoxy composites were predicted using the model formulated previously.²⁸ The theoretical percolation threshold, V_c , was calculated using the filler aspect ratio (D/t) and content ratio (V_1/V_2), as well as mean orientation factor, $\langle \cos^2 \theta \rangle$, which is measured as shown in Figure 3c,f. The percolation factor, R , was obtained using the following equation

$$R = \frac{(D + D_{IP})^3 \frac{V_1}{V_2} \langle \cos^2 \theta_1 \rangle^3 + \langle \cos^2 \theta_2 \rangle^3}{D^2 t \left(1 + \frac{V_1}{V_2} \right)} \quad (1)$$

where D and t refer to the size and thickness of GO sheets, respectively, whereas the interparticle distance, D_{IP} , is assumed to be 10 nm. V_c was determined according to eq 2

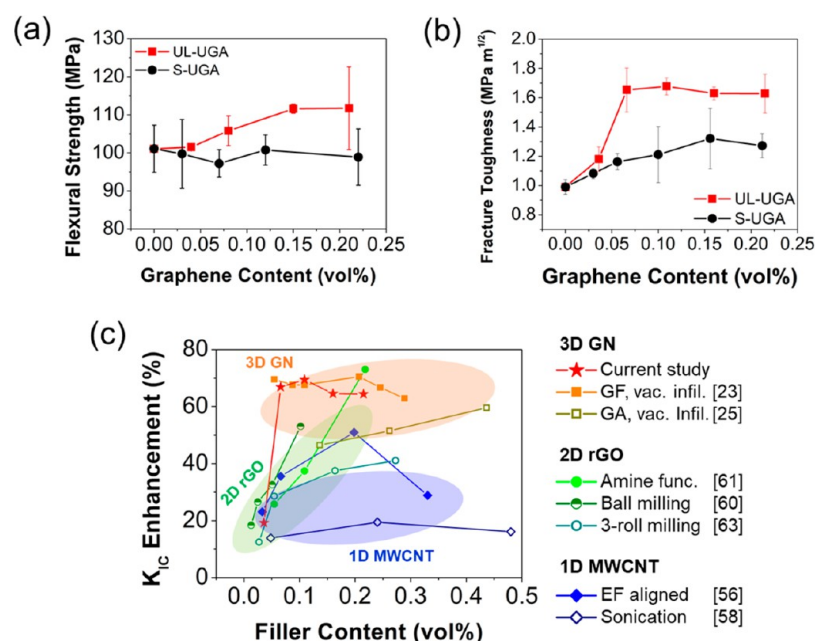


Figure 7. (a) Flexural strength and (b) mode I fracture toughness of UL-UGA and S-UGA/epoxy composites with graphene sheets aligned transverse to the loading direction. (c) Comparison of enhancements of fracture toughness, K_{1C} , between the UL-UGA/epoxy composites prepared in this study and selective carbon/epoxy nanocomposites reported in the literature.

$$V_c = \frac{\pi}{4} \left(\frac{1}{R} \right) \quad (2)$$

A summary of these values for UGA/epoxy composites is presented in Table S2. As UL-GO had a very high aspect ratio of 31 600 and was capable of producing a highly aligned UGA structure, it possessed high D/t , $\langle \cos^2 \theta_1 \rangle$, and V_1/V_2 values, giving rise to a high percolation factor and a low theoretical percolation. The predicted percolation thresholds were 0.198, 0.02, and 0.0044 vol % for S-UGA, L-UGA, and UL-UGA, respectively, which are in good agreement with the experimental results, as shown in Figure 6c. Here, the ordinate of each data point represents its experimental percolation threshold, whereas the abscissa shows the calculated percolation factor from eq 1. The straight line is a plot of eq 2, which describes the inverse relationship between theoretical percolation threshold and percolation factor. Slight differences between the experimental and theoretical results were expected, as there were irregularities in pore morphology of UGAs, overlapping of graphene, and wrinkling in large graphene sheets.

The comparison of percolation thresholds of representative carbon nanofiller/epoxy composites reported in the literature is shown in Table 1. For 0D CB, geometrical models predicted 16 vol % as the minimum filler volume fraction to form a percolated network.⁴⁹ However, CB/epoxy composites with lower percolation thresholds have been reported as a result of the tunneling effect and the formation of long interconnected networks of particles, called the “high structures”.^{50,51} Shear mixing or increasing the ionic concentration of CB/epoxy dispersion may induce the formation of such high structures, resulting in low percolation thresholds of 0.3 and 0.06 vol %, respectively.⁵⁰ Because of their high aspect ratios and electrical conductivities, 1D CNTs generally exhibited very low percolation thresholds, depending on CNT type, synthesis method, aspect ratio, and dispersion method.⁵² A pioneering study reported a percolation threshold of 0.02 vol % by

dispersing chemical vapor deposition (CVD)-grown MWCNTs in epoxy resin.⁵³ Shear-mixing aligned CVD-grown MWCNTs have shown the lowest percolation threshold of 0.0014 vol %, signifying the effect of filler alignment and dispersion method.⁵⁴ Despite the smaller diameters of single-walled CNTs (SWCNTs), the lowest percolation threshold reported, 0.0052 vol %, was higher than that of aligned MWCNTs because of their tendency to entangle.⁵⁵ Reduced graphene oxide (rGO) sheets are commonly used as 2D fillers owing to their high dispersability in liquid polymers, which enables in situ polymerization of epoxy to form composites with a low percolation threshold of 0.12 vol %.⁴⁵ Pristine graphene having a higher electrical conductivity than rGO was uniformly dispersed in epoxy by freeze-drying and mixing to achieve an even lower threshold of 0.088 vol %.²⁰ However, these 2D graphene sheets with high aspect ratios tended to agglomerate due to van der Waals forces,²⁰ resulting in higher percolation thresholds of the composites than the MWCNT counterparts. To address this issue, 2D graphene sheets have been rationally assembled to form 3D interconnected graphene networks that could maintain their 3D structure even after the infiltration of polymer resin. CVD-grown graphene foam (GF)/epoxy composites boasted an impressive percolation of 0.027 vol % with a high conductivity of 0.97 S/cm.²³ The two-step reduction and freeze-drying of GO sheets present a facile method of preparing 3D interconnected GAs with good mechanical flexibility, but resulted in a higher percolation threshold of 0.14 vol % due to inevitable agglomeration of GO sheets during the gelation process.²⁵ Direct freeze-drying of GO minimized the agglomeration problem through ice-template-directed assembly of graphene sheets. After subsequent thermal reduction, such aerogels exhibited ultralow densities lower than 0.3 mg/cm³ with an ultralow percolation threshold of 0.007 vol % of the composites.²⁸ The UGAs presented in this study were prepared using the same method, and the use of ultralarge graphene sheets further reduced the percolation threshold to a remarkable value 0.0066 vol %, which is among the lowest

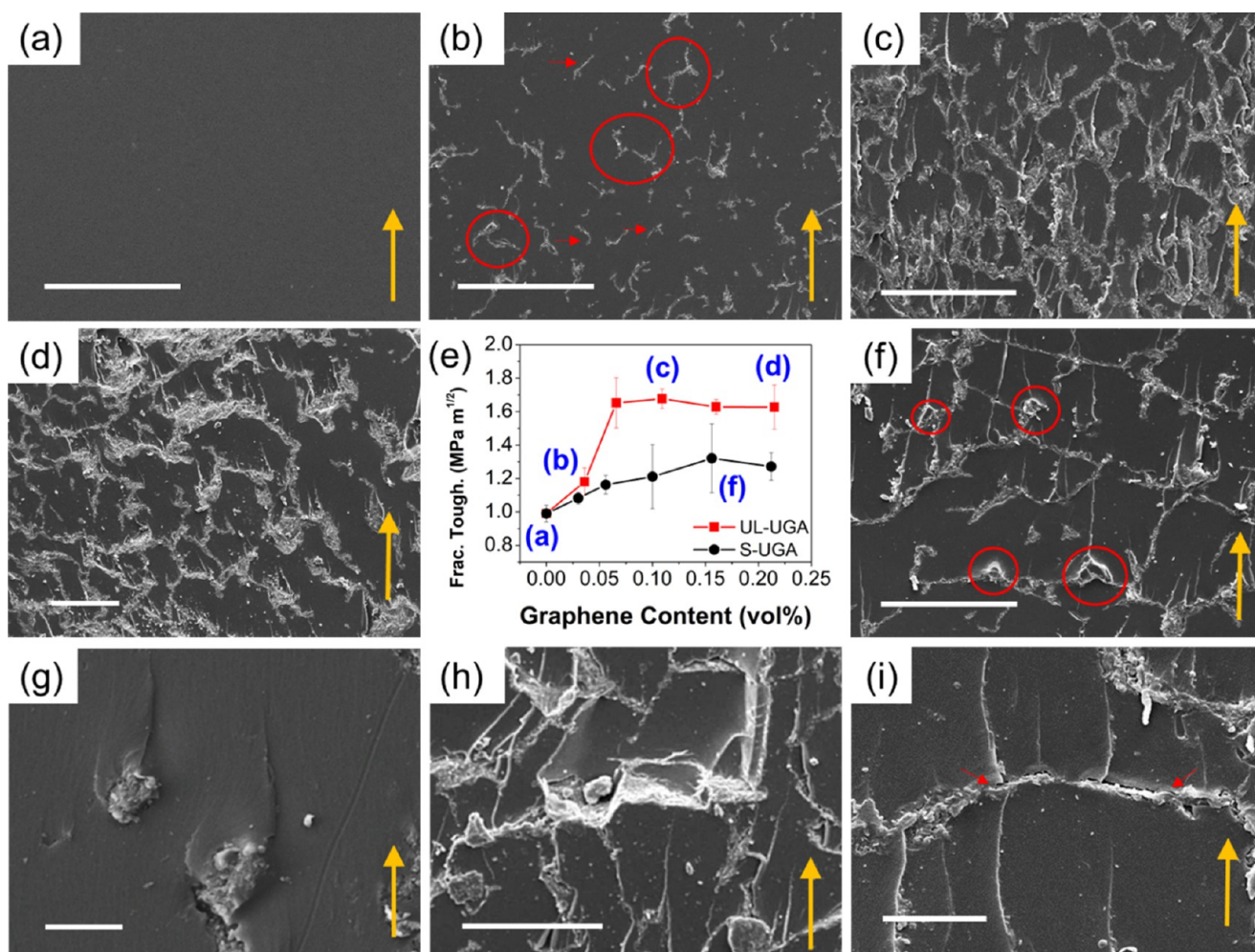


Figure 8. Typical SEM images of fracture surface for (a) neat epoxy and epoxy composites with (b) 0.04 vol %, (c) 0.11 vol %, and (d) 0.22 vol % UL-UGA aligned against the crack plane. (e) Mode I fracture toughness of UL-UGA and S-UGA/epoxy composites, indicating fracture toughness corresponding to each fracture surface. (f) SEM image of fracture surface of composite with 0.16 vol % S-UGA. Toughening mechanisms observed on the fracture surface of epoxy composites: (g) crack pinning and bifurcation at 0.04 vol %, (h) crack deflection with propagation on different plane at 0.07 vol %, and (i) void nucleation at debonded interface at 0.11 vol % of UL-UGA. The scale bars represent 100 μm in (a–f) and 10 μm in (g–i), the red arrows and circles indicate special features mentioned in text, whereas the large vertical arrows indicate the crack propagation direction.

values for carbon nanofiller/epoxy composites reported in the literature.

3.5. Mechanical Properties of UGA/Epoxy Composites. The modulus and strength of UGA/epoxy composites measured in three-point flexure are shown in Figures S8 and 7a, respectively. The flexural modulus of epoxy increased from 2.56 to 2.85 GPa at 0.2 vol % of S-UGA and to 2.87 GPa at 0.2 vol % of UL-UGA. Meanwhile, the flexural strength of UL-UGA composites increased to 112 MPa, which is equivalent to an 11% enhancement compared to the neat epoxy, at 0.15 vol %, and became saturated upon further increase in graphene content. In contrast, the addition of S-UGA fillers resulted in fluctuating flexural strengths despite the increase in flexural modulus because the low aspect ratio of S-GO resulted in less-effective load transfer than those containing UL-UGAs. Overall, the improvements in flexural properties were not impressive because good interfacial bonds between the UGA and epoxy are required to enhance these properties. The lack of functional groups on the graphene surface, as shown in the XPS images (Figure 5c), means that the UGAs could not form chemical bonds with the epoxy resin.^{25,58} The weak interaction at the interface is evident from the extensive debonding of graphene

sheets observed in the next section, which would limit the load transfer from the epoxy matrix to the graphene sheets.⁵⁹

Mode I fracture toughnesses, K_{IC} , of neat epoxy and the composites were measured in single-edge notched bending, and the results are given in Figure 7b. The fracture toughness of neat epoxy was 0.99 $\text{MPa m}^{1/2}$, which is consistent with previous reports for the same epoxy system.^{23,25} The fracture toughness of the composites, in which graphene sheets were perpendicular to the crack plane, increased with increasing filler content up to 1.68 $\text{MPa m}^{1/2}$ at 0.11 vol % of UL-UGA, 69% higher than the toughness of neat epoxy, followed by saturation at higher filler contents. Compared to UL-UGAs, S-UGAs were less effective in enhancing the fracture toughness of the composites for all graphene contents, showing a maximum toughness of 1.32 $\text{MPa m}^{1/2}$ at 0.16 vol %, 33% higher than that of neat epoxy. These results signify much more pronounced enhancements in fracture toughness than the enhancements in flexural properties. The fracture toughness of composites with the graphene sheets aligned along the crack propagation direction is shown in Figure S9. With UL-UGA fillers, the fracture toughness increased to 1.47 $\text{MPa m}^{1/2}$ at 0.11 vol %. However, a further increase in graphene content resulted in a

sharp reduction owing to the easy cleavage of aligned graphene sheets along the crack plane, much lower than those with cracks running transverse to alignment. For S-UGA fillers, the fracture toughness and fracture surface were similar for both crack orientations because the graphene sheets were rather randomly dispersed in the matrix.

The enhancement of fracture toughness K_{IC} due to UL-UGA was compared to that of representative carbon nanofillers reported in the literature, as shown in Figure 7c and Table S3. Among various 1D MWCNT processing techniques, dispersing CNTs into epoxy matrix by stirring and sonication presented a modest 19% enhancement in K_{IC} at 0.24 vol %, whereas a further increase in filler content resulted in a slight reduction in K_{IC} due to the local agglomeration of CNTs.⁵⁸ Epoxy composites with MWCNTs aligned by electric fields exhibited a higher K_{IC} enhancement of up to 51% at 0.2 vol % filler loading, which also suffered from the detrimental effects of CNT agglomeration at higher filler contents.⁵⁶ As for 2D graphene, ball-milling of rGO with epoxy resin resulted in an impressive 53% enhancement at 0.1 vol % loading.⁶⁰ Amine functionalization enabled uniform dispersion of rGO sheets at a high filler loading of 0.22 vol %, resulting in an exceptional 73% enhancement.⁶¹ The complex functionalization and dispersion techniques involved in achieving a uniform graphene dispersion may be avoided by preparing 3D graphene networks prior to epoxy infiltration. GA-reinforced epoxy composites with 0.44 vol % graphene loading showed a 60% higher K_{IC} than neat epoxy.²⁵ GFs prepared by CVD have shown to increase the K_{IC} of epoxy by 70% at a very low filler content of 0.06 vol %.²³ UL-UGAs, prepared using a facile and cost-effective freeze-drying method, were capable of producing a similar K_{IC} enhancement of 69% at 0.11 vol % filler content, owing to the various toughening mechanisms introduced by highly aligned ultralarge graphene sheets. In summary, 2D rGO sheets were more effective than 1D MWCNTs in toughening the epoxy matrix, but required rigorous functionalization and dispersion processes to achieve significant enhancements at high filler contents. Meanwhile, the 3D graphene network presents a unique approach to distribute aligned graphene sheets uniformly within the matrix, giving rise to exceptional toughness enhancement at low filler contents.

The SEM image shown in Figure 8a displays a smooth and featureless fracture surface for neat epoxy, typical of brittle materials with very weak resistance to crack propagation. The addition of graphene fillers enhanced the fracture toughness of epoxy by several toughening mechanisms, namely, crack pinning, crack deflection, crack bridging, filler rupture, and interfacial debonding.^{60,62,63} Such features produced characteristic rough fracture surface of toughened composites.^{23,25,62,63} For the composites with graphene sheets aligned transverse to the crack plane, SEM images taken of fracture surfaces of the composites at various filler contents of S-UGA and UL-UGA are shown in Figure S10. At a low UL-UGA content of 0.04 vol %, the fracture surface was relatively smooth (Figure 8b), featuring small regions of interconnected graphene networks, as indicated by the red circles, as well as individual graphene sheets, as indicated by the red arrows. The UGAs prepared using low-concentration GO sheets consisted of graphene sheets that were loosely interconnected at their edges. When these UGAs were used as fillers, the interconnections may not be present exactly at the crack plane. Thus, segregated graphene sheets, instead of a single interconnected graphene network, were observed on the fracture surface. Such isolated sheets were

able to toughen the epoxy matrix by crack pinning and bifurcation, as evidenced by crack front bowing and the formation of tails (Figure 8g).⁶² As a result, these composites displayed a 19% enhancement in fracture toughness compared to neat epoxy. In comparison, the composite with a higher UL-UGA content of 0.11 vol % featured a rough fracture surface with multiplane regions around 20–30 μm in size (Figure 8c), which is consistent with the UGA pore sizes observed in Figure 3a. These regions were separated by interconnected graphene sheets distributed across the epoxy matrix. As the propagating crack encounters a graphene sheet, the crack tip would be blunted and deflected along the boundaries of the graphene sheet, before resuming propagation on a different plane (Figure 8h). These crack deflections resulted in a tension-shear mixed mode fracture phenomenon with largely boosted fracture surface area, effectively enhancing the energy absorption of the composite.⁶⁴ In addition, the crack tip blunting process may induce the nucleation of voids at the graphene–epoxy interface, as shown between the red arrows in Figure 8i, contributing to a large fracture surface area and enhanced energy absorption of the composite.⁶³ These modifications to the crack propagation behavior resulted in a remarkable 69% enhancement in fracture toughness of epoxy. A further increase in filler content resulted in a slight reduction in fracture toughness, similar to a previous report for GF/epoxy composites.²³ The corresponding fracture surface (Figure 8d) presented extensive, flat areas between thick bundles of graphene sheets. The UGAs prepared with a very high UL-GO concentration of 4.0 mg/mL tended to have thick agglomerated pore walls, which failed to enhance the toughness with less-effective crack deflection and interfacial debonding. For S-UGA/epoxy composites, however, crack pinning by aggregated S-GO sheets was observed as the primary toughening mechanism across all filler contents, as indicated by the red circles in Figure 8f, but there were no signs of crack deflection.

4. CONCLUSIONS

The effects of GO sheet size on the electrical and mechanical properties of UGAs and UGA/epoxy composites were studied. A two-step centrifugation method was used to isolate GO dispersions according to their sheet sizes. Unidirectional freeze-casting of these sorted dispersions followed by thermal reduction produced UGAs, which were subsequently infiltrated with liquid epoxy resin under vacuum to produce UGA/epoxy composites. These composites exhibited unique anisotropic conductivities and size-dependent percolation thresholds, along with robust mechanical properties. In the wider scope, the results presented in this study may provide a guideline for the preparation of 3D porous networks from 2D graphene building blocks, supplementing previous reports.

It is found that the UGAs prepared using UL-GO had highly aligned pore walls with a high orientation factor, consisting of high-quality and low-defect graphene sheets, whereas the UGAs prepared using S-GO exhibited randomly oriented pore walls having apparently more defects. The UL-UGA/epoxy composites exhibited excellent electrical conductivity of 0.135 S/cm and an ultralow percolation threshold of 0.0066 vol % owing to their very high aspect ratio and alignment of UL-UGA. This is among the lowest threshold of carbon nanofiller/polymer composites reported in the literature. The experimental results were in close agreement with the theoretical values predicted by an interparticle distance model. The flexural strength and moduli of UGA/epoxy composites were limited by the weak

interfacial bonding. Nevertheless, UL-UGAs effectively enhanced the fracture toughness of epoxy by 69% at 0.11 vol % graphene content, arising from multiple toughening mechanisms, such as crack pinning, crack deflection, and interfacial debonding. Incidentally, a new approach has been recently proposed to enhance the fracture toughness of epoxy composites by compacting the CVD-grown GFs so as to achieve extremely high graphene content.⁶⁵

■ ASSOCIATED CONTENT

Supporting Information

The Supporting Information is available free of charge on the ACS Publications website at DOI: 10.1021/acsami.7b19069.

Schematic for UGA fabrication; supplementary UGA densities, XPS images, Raman spectra, mechanical properties, fracture surface; data processing techniques for GO size, graphene alignment, Raman spectra, and percolation threshold (PDF)

■ AUTHOR INFORMATION

Corresponding Author

*E-mail: mejkkm@ust.hk.

ORCID

Ne Myo Han: 0000-0001-9389-7141

Xi Shen: 0000-0003-1688-4931

Jang-Kyo Kim: 0000-0002-5390-8763

Notes

The authors declare no competing financial interest.

■ ACKNOWLEDGMENTS

The project was supported by the Research Grants Council (GRF Projects: 16203415, 16229216, and 16205517) of Hong Kong SAR. N.M.H. was a recipient of the Bai Xian Asian Future Leaders Scholarship, whereas Z.W. and X.S. were recipients of the Hong Kong Ph.D. Fellowship. Technical assistance from Materials Characterization and Preparation Facilities (MCPF), Advanced Engineering Materials Facilities (AEMF), Department of Chemical and Biomolecular Engineering, and Division of Biomedical Engineering at HKUST is appreciated.

■ REFERENCES

- (1) Yamada, T.; Hayamizu, Y.; Yamamoto, Y.; Yomogida, Y.; Izadi-Najafabadi, A.; Futaba, D. N.; Hata, K. A Stretchable Carbon Nanotube Strain Sensor for Human-Motion Detection. *Nat. Nanotechnol.* **2011**, *6*, 296–301.
- (2) Liu, X.; Tang, C.; Du, X.; Xiong, S.; Xi, S.; Liu, Y.; Shen, X.; Zheng, Q. B.; Wang, Z.; Wu, Y.; Horner, A.; Kim, J. K. A Highly Sensitive Graphene Woven Fabric Strain Sensor for Wearable Wireless Musical Instruments. *Mater. Horiz.* **2017**, *4*, 477–486.
- (3) Wu, S.; Zhang, J.; Ladani, R. B.; Ravindran, A. R.; Mouritz, A. P.; Kinloch, A. J.; Wang, C. H. Novel Electrically Conductive Porous PDMS/Carbon Nanofiber Composites for Deformable Strain Sensors and Conductors. *ACS Appl. Mater. Interfaces* **2017**, *9*, 14207–14215.
- (4) Baughman, R. H.; Cui, C.; Zakhidov, A. A.; Iqbal, Z.; Barisci, J. N.; Spinks, G. M.; Wallace, G. G.; Mazzoldi, A.; De Rossi, D.; Rinzler, A. G.; Jaszchinski, O.; Roth, S.; Kertesz, M. Carbon Nanotube Actuators. *Science* **1999**, *284*, 1340–1344.
- (5) Li, C.; Thostenson, E. T.; Chou, T. Sensors and Actuators Based on Carbon Nanotubes and their Composites: A Review. *Compos. Sci. Technol.* **2008**, *68*, 1227–1249.
- (6) Landi, B. J.; Raffaele, R. P.; Heben, M. J.; Alleman, J. L.; VanDerveer, W.; Gennett, T. Single Wall Carbon Nanotube–Nafion Composite Actuators. *Nano Lett.* **2002**, *2*, 1329–1332.
- (7) Gurunathan, K.; Murugan, A. V.; Marimuthu, R.; Mulik, U.; Amalnerkar, D. Electrochemically Synthesised Conducting Polymeric Materials for Applications Towards Technology in Electronics, Optoelectronics and Energy Storage Devices. *Mater. Chem. Phys.* **1999**, *61*, 173–191.
- (8) Barber, P.; Balasubramanian, S.; Anguchamy, Y.; Gong, S.; Wibowo, A.; Gao, H.; Ploehn, H. J.; Zur Loye, H. Polymer Composite and Nanocomposite Dielectric Materials for Pulse Power Energy Storage. *Materials* **2009**, *2*, 1697–1733.
- (9) Sun, X.; Liu, X.; Shen, X.; Wu, Y.; Wang, Z.; Kim, J. K. Graphene Foam/Carbon Nanotube/Poly (Dimethyl Siloxane) Composites for Exceptional Microwave Shielding. *Composites, Part A* **2016**, *85*, 199–206.
- (10) Wu, Y.; Wang, Z.; Liu, X.; Shen, X.; Zheng, Q. B.; Xue, Q.; Kim, J. K. Ultralight Graphene Foam/Conductive Polymer Composites for Exceptional Electromagnetic Interference Shielding. *ACS Appl. Mater. Interfaces* **2017**, *9*, 9059–9069.
- (11) Zeng, Z.; Chen, M.; Jin, H.; Li, W.; Xue, X.; Zhou, L.; Pei, Y.; Zhang, H.; Zhang, Z. Thin and Flexible Multi-Walled Carbon Nanotube/Waterborne Polyurethane Composites with High-Performance Electromagnetic Interference Shielding. *Carbon* **2016**, *96*, 768–777.
- (12) Eda, G.; Chhowalla, M. Graphene-Based Composite Thin Films for Electronics. *Nano Lett.* **2009**, *9*, 814–818.
- (13) Gaynor, W.; Burkhard, G. F.; McGehee, M. D.; Peumans, P. Smooth Nanowire/Polymer Composite Transparent Electrodes. *Adv. Mater.* **2011**, *23*, 2905–2910.
- (14) Balberg, I. A Comprehensive Picture of the Electrical Phenomena in Carbon Black–polymer Composites. *Carbon* **2002**, *40*, 139–143.
- (15) Hindermann-Bischoff, M.; Ehrburger-Dolle, F. Electrical Conductivity of Carbon Black–polyethylene Composites: Experimental Evidence of the Change of Cluster Connectivity in the PTC Effect. *Carbon* **2001**, *39*, 375–382.
- (16) Mondal, S.; Ganguly, S.; Das, P.; Khastgir, D.; Das, N. C. Low Percolation Threshold and Electromagnetic Shielding Effectiveness of Nano-Structured Carbon Based Ethylene Methyl Acrylate Nanocomposites. *Composites, Part B* **2017**, *119*, 41–56.
- (17) Li, J.; Ma, P. C.; Chow, W. S.; To, C. K.; Tang, B. Z.; Kim, J. K. Correlations between Percolation Threshold, Dispersion State, and Aspect Ratio of Carbon Nanotubes. *Adv. Funct. Mater.* **2007**, *17*, 3207–3215.
- (18) Li, C.; Thostenson, E. T.; Chou, T. Dominant Role of Tunneling Resistance in the Electrical Conductivity of Carbon Nanotube–based Composites. *Appl. Phys. Lett.* **2007**, *91*, No. 223114.
- (19) Ma, P.-C.; Liu, M.; Zhang, H.; Wang, S.; Wang, R.; Wang, K.; Wong, Y.; Tang, B.; Hong, S.; Paik, K. Enhanced Electrical Conductivity of Nanocomposites Containing Hybrid Fillers of Carbon Nanotubes and Carbon Black. *ACS Appl. Mater. Interfaces* **2009**, *1*, 1090–1096.
- (20) Wajid, A. S.; Ahmed, H.; Das, S.; Irin, F.; Jankowski, A. F.; Green, M. J. High-Performance Pristine Graphene/Epoxy Composites with Enhanced Mechanical and Electrical Properties. *Macromol. Mater. Eng.* **2013**, *298*, 339–347.
- (21) Yousefi, N.; Sun, X.; Lin, X.; Shen, X.; Jia, J. J.; Zhang, B.; Tang, B. Z.; Chan, M. S.; Kim, J. K. Highly Aligned Graphene/Polymer Nanocomposites with Excellent Dielectric Properties for High-performance Electromagnetic Interference Shielding. *Adv. Mater.* **2014**, *26*, 5480–5487.
- (22) Chen, Z.; Xu, C.; Ma, C.; Ren, W.; Cheng, H. M. Lightweight and Flexible Graphene Foam Composites for High-performance Electromagnetic Interference Shielding. *Adv. Mater.* **2013**, *25*, 1296–1300.
- (23) Jia, J.; Sun, X.; Lin, X.; Shen, X.; Mai, Y.; Kim, J. K. Exceptional Electrical Conductivity and Fracture Resistance of 3D Interconnected Graphene Foam/Epoxy Composites. *ACS Nano* **2014**, *8*, 5774–5783.
- (24) Tang, G.; Jiang, Z.; Li, X.; Zhang, H.; Dasari, A.; Yu, Z. Z. Three Dimensional Graphene Aerogels and their Electrically Conductive Composites. *Carbon* **2014**, *77*, 592–599.

- (25) Wang, Z.; Shen, X.; Akbari Garakani, M.; Lin, X.; Wu, Y.; Liu, X.; Sun, X.; Kim, J. K. Graphene Aerogel/Epoxy Composites with Exceptional Anisotropic Structure and Properties. *ACS Appl. Mater. Interfaces* **2015**, *7*, 5538–5549.
- (26) Worsley, M. A.; Pauzauskis, P. J.; Olson, T. Y.; Biener, J.; Satcher, J. H., Jr.; Baumann, T. F. Synthesis of Graphene Aerogel with High Electrical Conductivity. *J. Am. Chem. Soc.* **2010**, *132*, 14067–14069.
- (27) Sun, H.; Xu, Z.; Gao, C. Multifunctional, Ultra-flyweight, Synergistically Assembled Carbon Aerogels. *Adv. Mater.* **2013**, *25*, 2554–2560.
- (28) Wang, Z.; Shen, X.; Han, N. M.; Liu, X.; Wu, Y.; Ye, W.; Kim, J. K. Ultralow Electrical Percolation in Graphene Aerogel/Epoxy Composites. *Chem. Mater.* **2016**, *28*, 6731–6741.
- (29) Xie, X.; Zhou, Y.; Bi, H.; Yin, K.; Wan, S.; Sun, L. Large-Range Control of the Microstructures and Properties of Three-Dimensional Porous Graphene. *Sci. Rep.* **2013**, *3*, No. 2117.
- (30) Wu, S.; Ladani, R. B.; Zhang, J.; Ghorbani, K.; Zhang, X.; Mouritz, A. P.; Kinloch, A. J.; Wang, C. H. Strain Sensors with Adjustable Sensitivity by Tailoring the Microstructure of Graphene Aerogel/PDMS Nanocomposites. *ACS Appl. Mater. Interfaces* **2016**, *8*, 24853–24861.
- (31) Zheng, Q. B.; Ip, W. H.; Lin, X.; Yousefi, N.; Yeung, K. K.; Li, Z.; Kim, J. K. Transparent Conductive Films Consisting of Ultralarge Graphene Sheets Produced by Langmuir–Blodgett Assembly. *ACS Nano* **2011**, *5*, 6039–6051.
- (32) Lin, X.; Shen, X.; Zheng, Q. B.; Yousefi, N.; Ye, L.; Mai, Y.; Kim, J. K. Fabrication of Highly-Aligned, Conductive, and Strong Graphene Papers using Ultralarge Graphene Oxide Sheets. *ACS Nano* **2012**, *6*, 10708–10719.
- (33) Yousefi, N.; Gudarzi, M. M.; Zheng, Q. B.; Aboutalebi, S. H.; Sharif, F.; Kim, J. K. Self-Alignment and High Electrical Conductivity of Ultralarge Graphene Oxide–polyurethane Nanocomposites. *J. Mater. Chem.* **2012**, *22*, 12709–12717.
- (34) Kim, J.; Kim, J.; Song, S.; Zhang, S.; Cha, J.; Kim, K.; Yoon, H.; Jung, Y.; Paik, K.; Jeon, S. W. Strength Dependence of Epoxy Composites on the Average Filler Size of Non-Oxidized Graphene Flake. *Carbon* **2017**, *113*, 379–386.
- (35) Qin, Z.; Jung, G. S.; Kang, M. J.; Buehler, M. J. The Mechanics and Design of a Lightweight Three-Dimensional Graphene Assembly. *Sci. Adv.* **2017**, *3*, No. e1601536.
- (36) Bai, H.; Li, C.; Wang, X.; Shi, G. On the Gelation of Graphene Oxide. *J. Phys. Chem. C* **2011**, *115*, 5545–5551.
- (37) Jia, J. J.; Kan, C. M.; Lin, X.; Shen, X.; Kim, J. K. Effects of Processing and Material Parameters on Synthesis of Monolayer Ultralarge Graphene Oxide Sheets. *Carbon* **2014**, *77*, 244–254.
- (38) Deville, S.; Meille, S.; Seuba, J. A Meta-Analysis of the Mechanical Properties of Ice-Templated Ceramics and Metals. *Sci. Technol. Adv. Mater.* **2015**, *16*, No. 043501.
- (39) Bryning, M. B.; Millie, D. E.; Islam, M. F.; Hough, L. A.; Kikkawa, J. M.; Yodh, A. G. Carbon Nanotube Aerogels. *Adv. Mater.* **2007**, *19*, 661–664.
- (40) Xu, Z.; Zhang, Y.; Li, P.; Gao, C. Strong, Conductive, Lightweight, Neat Graphene Aerogel Fibers with Aligned Pores. *ACS Nano* **2012**, *6*, 7103–7113.
- (41) Casabianca, L. B.; Shaibat, M. A.; Cai, W. W.; Park, S.; Piner, R.; Ruoff, R. S.; Ishii, Y. NMR-Based Structural Modeling of Graphite Oxide using Multidimensional 13C Solid-State NMR and Ab Initio Chemical Shift Calculations. *J. Am. Chem. Soc.* **2010**, *132*, 5672–5676.
- (42) Sing, K. S. Reporting Physisorption Data for Gas/Solid Systems with Special Reference to the Determination of Surface Area and Porosity. *Pure Appl. Chem.* **1985**, *57*, 603–619.
- (43) Yang, D.; Velamakanni, A.; Bozoklu, G.; Park, S.; Stoller, M.; Piner, R. D.; Stankovich, S.; Jung, I.; Field, D. A.; Ventrice, C. A.; et al. Chemical Analysis of Graphene Oxide Films After Heat and Chemical Treatments by X-Ray Photoelectron and Micro-Raman Spectroscopy. *Carbon* **2009**, *47*, 145–152.
- (44) King, A. A.; Davies, B. R.; Noorbehesht, N.; Newman, P.; Church, T. L.; Harris, A. T.; Raza, J. M.; Minett, A. I. A New Raman Metric for the Characterisation of Graphene Oxide and its Derivatives. *Sci. Rep.* **2016**, *6*, No. 19491.
- (45) Yousefi, N.; Lin, X.; Zheng, Q. B.; Shen, X.; Pothnis, J. R.; Jia, J.; Zussman, E.; Kim, J. K. Simultaneous in Situ Reduction, Self-Alignment and Covalent Bonding in Graphene Oxide/Epoxy Composites. *Carbon* **2013**, *59*, 406–417.
- (46) Gao, J.; Yan, D.; Yuan, B.; Huang, H.; Li, Z. Large-Scale Fabrication and Electrical Properties of an Anisotropic Conductive Polymer Composite Utilizing Preferable Location of Carbon Nanotubes in a Polymer Blend. *Compos. Sci. Technol.* **2010**, *70*, 1973–1979.
- (47) Li, X.; Li, X.; Liao, K.; Min, P.; Liu, T.; Dasari, A.; Yu, Z. Z. Thermally Annealed Anisotropic Graphene Aerogels and their Electrically Conductive Epoxy Composites with Excellent Electromagnetic Interference Shielding Efficiencies. *ACS Appl. Mater. Interfaces* **2016**, *8*, 33230–33239.
- (48) Zeng, Z.; Jin, H.; Chen, M.; Li, W.; Zhou, L.; Zhang, Z. Lightweight and Anisotropic Porous MWCNT/WPU Composites for Ultrahigh Performance Electromagnetic Interference Shielding. *Adv. Funct. Mater.* **2016**, *26*, 303–310.
- (49) Kirkpatrick, S. Percolation Phenomena in Higher Dimensions: Approach to the Mean-Field Limit. *Phys. Rev. Lett.* **1976**, *36*, 69–72.
- (50) Schueler, R.; Petermann, J.; Schulte, K.; Wentzel, H.-P. Agglomeration and Electrical Percolation Behavior of Carbon Black Dispersed in Epoxy Resin. *J. Appl. Polym. Sci.* **1997**, *63*, 1741–1746.
- (51) El-Tantawy, F.; Kamada, K.; Ohnabe, H. In situ Network Structure, Electrical and Thermal Properties of Conductive Epoxy Resin–Carbon Black Composites for Electrical Heater Applications. *Mater. Lett.* **2002**, *56*, 112–126.
- (52) Bauhofer, W.; Kovacs, J. Z. A Review and Analysis of Electrical Percolation in Carbon Nanotube Polymer Composites. *Compos. Sci. Technol.* **2009**, *69*, 1486–1498.
- (53) Sandler, J.; Shaffer, M. S. P.; Prasse, T.; Bauhofer, W.; Shulte, K.; Windle, A. H. Development of a Dispersion Process for Carbon Nanotubes in an Epoxy Matrix and the Resulting Electrical Properties. *Polymer* **1999**, *40*, 5967–5971.
- (54) Martin, C. A.; Sandler, J. K. W.; Shaffer, M. S. P.; Schwarz, M. K.; Bauhofer, W.; Schulte, K.; Windle, A. H. Formation of Percolating Networks in Multi-Wall Carbon-Nanotube–epoxy Composites. *Compos. Sci. Technol.* **2004**, *64*, 2309–2316.
- (55) Bryning, M. B.; Islam, M. F.; Kikkawa, J. M.; Yodh, A. G. Very Low Conductivity Threshold in Bulk Isotropic Single-Walled Carbon Nanotube-Epoxy Composites. *Adv. Mater.* **2005**, *17*, 1186–1191.
- (56) Khan, S. U.; Pothnis, J. R.; Kim, J. K. Effects of Carbon Nanotube Alignment on Electrical and Mechanical Properties of Epoxy Nanocomposites. *Composites, Part A* **2013**, *49*, 26–34.
- (57) Liang, J.; Wang, Y.; Huang, Y.; Ma, Y.; Liu, Z.; Cai, J.; Zhang, C.; Gao, H.; Chen, Y. Electromagnetic Interference Shielding of Graphene/Epoxy Composites. *Carbon* **2009**, *47*, 922–925.
- (58) Saboori, B.; Ayatollahi, M. R. Experimental Fracture Study of MWCNT/Epoxy Nanocomposites Under the Combined Out-of-Plane Shear and Tensile Loading. *Polym. Test.* **2017**, *59*, 193–202.
- (59) Rafiee, M. A.; Rafiee, J.; Wang, Z.; Song, H.; Yu, Z. Z.; Koratkar, N. Enhanced Mechanical Properties of Nanocomposites at Low Graphene Content. *ACS Nano* **2009**, *3*, 3884–3890.
- (60) Tang, L. C.; Wan, Y. J.; Yan, D.; Pei, Y. B.; Zhao, L.; Li, Y. B.; Wu, L. B.; Jiang, J. X.; Lai, G. Q. The Effect of Graphene Dispersion on the Mechanical Properties of Graphene/Epoxy Composites. *Carbon* **2013**, *60*, 16–27.
- (61) Fang, M.; Zhang, Z.; Li, J.; Zhang, H.; Lu, H.; Yang, Y. Constructing Hierarchically Structured Interphases for Strong and Tough Epoxy Nanocomposites by Amine-Rich Graphene Surfaces. *J. Mater. Chem.* **2010**, *20*, 9635–9643.
- (62) Bortz, D. R.; Heras, E. G.; Martin-Gullon, I. Impressive Fatigue Life and Fracture Toughness Improvements in Graphene Oxide/Epoxy Composites. *Macromolecules* **2012**, *45*, 238–245.
- (63) Chandrasekaran, S.; Sato, N.; Tölle, F.; Mülhaupt, R.; Fiedler, B.; Schulte, K. Fracture Toughness and Failure Mechanism of Graphene Based Epoxy Composites. *Compos. Sci. Technol.* **2014**, *97*, 90–99.

(64) Rafiee, M. A.; Rafiee, J.; Srivastava, I.; Wang, Z.; Song, H.; Yu, Z. Z.; Koratkar, N. Fracture and Fatigue in Graphene Nanocomposites. *Small* **2010**, *6*, 179–183.

(65) Shen, X.; Wang, Z.; Wu, Y.; Liu, X.; He, Y. B.; Zheng, Q. B.; Yang, Q. H.; Kang, F.; Kim, J. K. Three-dimensional Multilayer Web for Polymer Nanocomposites with Exceptional Transport Properties and Fracture Resistance. *Mater. Horiz.* **2018**. [10.1039/C7MH00984D](https://doi.org/10.1039/C7MH00984D).